CrystEngComm

Accepted Manuscript

ROYAL SOCIETY OF CHEMISTRY

www.rsc.org/crystengcomm

Journal Name

RSCPublishing

ARTICLE

Crystal growth and characterization of thulium calcium oxyborate high temperature piezoelectric crystals

Cite this: DOI: 10.1039/x0xx00000x

Shuai Hou[a], Fapeng Yu*[ad], Yanqing Liu[a], Shujun Zhang[b], Qingming Lu[c], Shenglai Wang[a], Xian Zhao*[ad]

Received 00th January 2012,
Accepted 00th January 2012

DOI: 10.1039/x0xx00000x

www.rsc.org/

New rare-earth calcium oxyborate crystals $TmCa_4O(BO_3)_3$ (TmCOB) were grown by using the Czochralski pulling method, the mechanical and thermal properties were investigated. In addition, the dielectric, elastic and piezoelectric performances were evaluated by impedance method, where the piezoelectric charge coefficients were determined to be on the order of d_{11}=1.7, d_{12}=3.8, d_{13}=-4.2, d_{15}=-0.92, d_{24}=4.9, d_{26}=7.8, d_{31}=-0.75, d_{32}=-2.4, d_{33}=2.2 and d_{35}=-5.2 pC/N. The temperature dependent electrical resistivity and electro-elastic properties were studied from room temperature to 900°C, where high electrical resistivity of ~$6\times10^7\Omega\cdot$cm and low dielectric loss ~21% were achieved at 900°C, with high thermal stability of electromechanical coupling factors and piezoelectric coefficients over the temperature range of 20°C-900°C. All these properties demonstrate TmCOB crystals attractive candidate for high temperature sensor fabrications.

I Introduction

High temperature piezoelectric sensors are desirable in aerospace, automotive and energy industries etc., where the operational temperatures above 500°C are often required, hence, high temperature piezoelectric materials with the merits of high electrical resistivity, low dielectric loss, high piezoelectric coefficient and high thermal stability of piezoelectric and electromechanical properties over a wide temperature range are desirable for sensor fabrication. [1-7]

Comparing to ferroelectric ceramics, piezoelectric single crystals with no phase transition (or high Curie temperature point) are attractive for high temperature piezoelectric sensor fabrications, due to their advantages of high resistivity, low dielectric loss and reasonable piezoelectric properties at elevated temperatures. Among the piezoelectric crystal materials, the conventional quartz (α-SiO_2) was reported to possess high electrical resistivity, high mechanical quality factor (Q_m) and high temperature stability of resonance frequency, being widely used for piezoelectric resonator, filter and microbalance applications, however, its usage was restricted by crystal twinning and phase transition (α-β), being lower than 350°C.[1] Langasite family crystals (with ordered and disordered structures) are another type high temperature piezoelectric materials, which were reported to exhibit no phase transition prior to their respective melting points (1350°C -1500°C), high electrical resistivity (10^4-$10^6\Omega\cdot$cm @900°C) and piezoelectric coefficient (d_{11}= 4-7pC/N). However, further implementations were restricted due to the costly raw materials (Ga_2O_3).[8-12] Recently, noncentrosymmetric oxyborate single crystals have been studied for nonlinear, acoustically induced optical and piezoelectric applications.[13-17] Among these crystals, rare-earth calcium oxyborate crystals $ReCa_4O(BO_3)_3$ (ReCOB, Re: rare-earth elements) have attracted lots of interests for ultrahigh temperature piezoelectric applications. These crystals can be readily grown by Czockralski pulling method[18-23] and were reported to possess high electrical resistivity, low dielectric loss and strong electromechanical properties at elevated temperatures.[24-29] The effective piezoelectric coefficient (d'_{33}) of ReCOB crystals was found to be on the order of 5-6pC/N, comparable to that of langasite, while the electrical resistivities (YCOB and GdCOB), being on the order of $>10^7\Omega\cdot$cm at 900°C, 1-3 orders higher than langasite family crystals, exhibiting the advantages for ultrahigh temperature sensor applications.

In our previous studies on ReCOB crystals, the dielectric constant $\varepsilon^T_{22}/\varepsilon_0$, elastic compliance s^E_{66}, electromechanical coupling factor k_{26}, and piezoelectric coefficient d_{26} were found to increase with increasing Re^{3+} radius, with the maximum values being observed for PrCOB ($r^{Pr(+3)}$=0.990Å) crystals.[24, 29] However, ErCOB and YCOB crystals with smaller rare-earth ionic radius ($r^{Er(+3)}$ =0.883Å and $r^{Y(+3)}$ =0.890Å) were found to possess low dielectric and piezoelectric properties, but relative high electrical resistivity, high mechanical Q_m.[30] The Re^{3+} ions were believed to be the key factor dominating the electrical, dielectric, and piezoelectric properties of ReCOB crystals, which provides us an important clue to optimize and design new ReCOB crystals with comprehensive electro-elastic properties at elevated temperatures for piezoelectric applications, the purpose of this work.

II Experimental Section

2.1 Polycrystalline compounds synthesis

High purity (4N) $CaCO_3$, Re_2O_3 (Re: Yb, Lu and Tm) and H_3BO_3 powder were weighed in stoichiometric proportions for polycrystalline compounds preparation. The starting materials were fully mixed, pressed into tablets and calcinated at 1000°C in furnace (Si-Mo bar as the heater) for >5hrs to decompose the carbonates. The heating rate was controlled to be lower than 100°C/h to decrease

the evaporation of B_2O_3 during calcination process. After calcination, the formed oxides were ground, re-mixed and pressed into pieces, then put into high temperature furnace for solid-state reaction. The mixtures were sintered at 1200°C for 12hrs and then slowly cooling down to room temperature (RT) within 15-20hrs. The synthesized polycrystalline materials were kept in a dryer preparing for the single crystal growth.

2.2 Single crystal growth

Single crystal growth was carried out by conventional RF-heating (3kHz) Cz method using TDL-J40 furnace. An iridium crucible with 60.0mm in diameter and 35.0mm in depth was used for single crystal growth. The atmosphere in furnace was kept to be a mixture of N_2 (~98.0vol%) plus a small amount of O_2 (~2.0vol%), in order to protect the iridium crucible against oxidation. Initially, an <010>-orientated YCOB crystal seed was selected for small size TmCOB crystal growth, due to its high melting point around ~1510°C. Before seeding, the TmCOB melt was kept at 50-80°C above its melting point, then cooling down (~10°C/h) to a low temperature approximate about ~20°C above its melting point, at which, the YCOB seed maintained the same diameter. After soaking for half hour to form a new atomic interface at the end of crystal seed, pulling process was started for single crystal growth. Particularly, at the early necking stage, relative high pulling speed (3.0-5.0mm/h) and high rotation rate (20-25rpm) were utilized in order to get rid of the polycrystalline components along the YCOB seed. Particularly, the as-pulled seed from the melt was partly dissolved and continuously grown repeatedly, which we call it "seed-elimination" method, to get a short period of transparent TmCOB seed with minimal inclusions. Low pulling speed ranged from 0.5mm/h to 0.8 mm/h and moderate cooling speed (0.3-2.0°C/h) were applied during the shouldering process, until reached the desired crystal diameter (20-25mm), then the growing TmCOB crystal was pulled with a speed of 0.5 mm/h under a nearly constant temperature, depending on the designed thermal profile. After reaching the expected crystal length, the as-grown TmCOB crystal was pulled out of the melt and then cooled down to room temperature with a rate of 15.0-50.0°C/h.

2.3 Crystal structure analysis

Crystal structure was studied by using X-ray powder diffraction (XRPD) with a D8 Advance diffractometer (Bruker AXS, Advanced X-ray Solutions) equipped with Cu-Kα radiation (λ=0.15406 nm) and graphite monochromatorin a 2θ range of 10.0°-60.0°. The lattice parameters were calculated and refined by using SHELXL-97 system. The crystal densities were determined by the lattice parameters and the Archimedes method at ambient temperature of 25°C.

2.4 Thermal property measurement

Thermal expansion coefficients were measured by using a thermal dilatometer (Diamond TMA, Perkin-Elmer) with a heating rate of 5°C/min from 25°C to 500°C. Specific heat, thermal diffusion coefficients and thermal conductivities along the physical *X*-, *Y*- and *Z*- axes were measured using a Netzsch Nanoflash model LFA 457 apparatus by the laser pulse method over the temperature range of 20°C-700°C. The tested *X*-cut, *Y*-cut and *Z*-cut square wafers were prepared with dimension of 4.00×4.00×1.50mm^3, and the opposite surfaces were coated with graphite for measurement.

2.5 Electrical resistivity and electro-elasticproperty evaluation

The electrical resistivity was measured for the *X*-, *Y*- and *Z*-square crystal cuts in the temperature range of 500°C-900°C, using Tektronix DMM 4040 Digital Multimeter. The electro-elastic properties, including the dielectric constant, elastic compliances, electromechanical coupling factors and piezoelectric coefficients, were evaluated by impedance method (Agilent 4263B and HP4194A impedance/Gain-Phase Analyzer). Different crystal cuts (square plates, rectangular plates and rods) were designed and prepared according to the IEEE standard on piezoelectricity,[31] with dimensional ratio *t*(thickness):*w*(width):*l*(length) being on the order of 1.0:(6.0-7.0):(6.0-7.0), 1.0:(2.5-2.8):(8.0-9.0), and 1.0:1.0:(3.5-4.0) for square plates, rectangular plates and rods, respectively.

III. Results and Discussion

3.1 Polycrystalline compounds synthesis

For purpose of exploring new ReCOB crystals with higher electrical resistivity and lower dielectric loss than the reported YCOB and ErCOB crystals,[30] new ReCOB crystals with smaller Re radius, including TmCOB, YbCOB, and LuCOB, were selected. After mixing and calcination at 1200°C for 10hrs, TmCOB, YbCOB and LuCOB crystal phases were detected, where strong refractive peaks were observed for (130), (021) and (150) planes (Fig.1(a)), similar to the YCOB crystals, indicating the TmCOB, YbCOB, and LuCOB crystal phases are achievable, potential for single crystal growth. Nevertheless, YbCOB was found to be much harder to crystallize from the melt by using the Cz method than TmCOB, due to the incongruent melting behavior or narrow congruent melting region of the YbCOB melts, while LuCOB crystals can be crystallized by using the flux method (lead oxide as agent).[32] Considering the incongruent melting behavior or narrow congruent melting region of the YbCOB and the costly LuCOB components, TmCOB was designed for the single crystal growth.

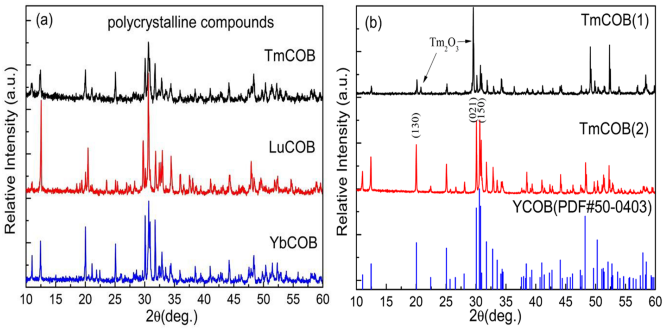

Fig.1 XRPD characterization for ReCOB (Re: Yb, Lu and Tm) polycrystalline compounds (a) and TmCOB crystals (b), in which the TmCOB(1) and TmCOB(2) data are obtained from samples in the Fig.2(a) and Fig.2(d), respectively.)

3.2 Single crystal growth

Using the YCOB crystal seeds, it was very difficult to get TmCOB single crystals at the first several runs, though the YCOB seed was dipped in the melts for several hours to reach solid-liquid interface equilibrium. The pulled polycrystalline blocks were observed to consist of a large number of small pores, as presented in Fig. 2(a).

The opaque polycrystalline block was found to be consisted of TmCOB and Tm_2O_3 phases, detected by the XRPD method (Fig. 1(b)-TmCOB(1)). The observed Tm_2O_3 phase indicated the components deviation from the real stoichiometry of the melt, induced by the evaporation of B_2O_3 during the solid-state reaction and crystal growth processes, leading to the excess of Tm_2O_3 in the melt, since the components were mixed in stoichiometric ratio. Therefore, excess H_3BO_3 (3-4wt%) was added to the stoichiometric raw materials for polycrystalline compound synthesis and single crystal growth.

The crystalline behaviour of the melts was greatly improved after component adjustment. However, crystal cracks and fiber-like inclusions were observed in TmCOB crystals at the beginning (Fig. 2(b)), where the excess H_3BO_3 was 2-3wt%. The fiber-like inclusions were found to be located near the middle-low part of the TmCOB crystal (Fig.2(c)), this phenomenon was also observed in Cz grown YCOB crystals,[21] which were found to be reduced by lowering the pulling speed after shouldering process and the compensation of B_2O_3 component in the melt.

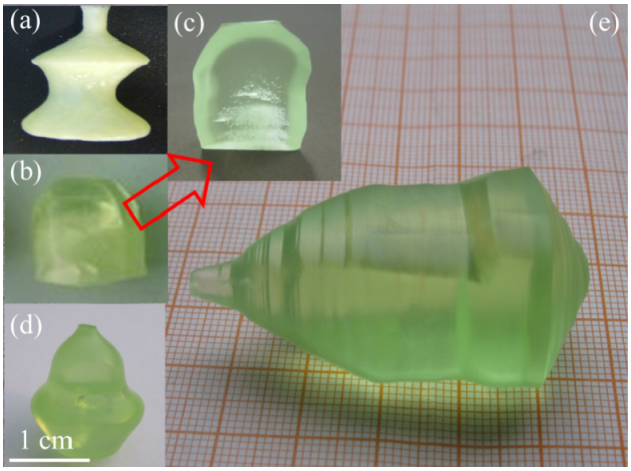

Fig. 2 Photographs of polycrystalline TmCOB materials and single crystals pulling along *Y*-axis((a) the pulled polycrystalline compounds, (b) TmCOB crystal with inclusions, (c) longitudinal section of crystal (b), (d) small TmCOB single crystal, and (e) large and high quality TmCOB single crystal)

Fig. 2(d) gives a small TmCOB single crystal free of inclusions after component adjustment, where the ingredients were modified with excess H_3BO_3 of 3-4wt%. The as-grown small TmCOB crystal bulk was then orientated and cut to seeds for the following large and high quality single crystal growth. Fig. 2(e) presents the as-grown transparent TmCOB single crystal free of inclusions and crystal cracks, with habitual faces (-201) and (101) being observed. Experimental results indicated that the congruent region of TmCOB crystals was very narrow, where the excess levels of H_3BO_3<3.0wt% or > 4wt% would be detrimental to high quality single crystal growth.

3.3 Crystal structure and density

The phase and lattice parameters of TmCOB single crystals were determined by XRPD method, results were given in Fig. 1(b)-TmCOB(2), where strong diffraction peaks were observed for (130), (220), and (150) planes, with diffraction angles (θ) being on the order of 20.046°, 25.076°, and 30.074°, respectively, close to those of YCOB crystals (PDF#50-0403), indicating the TmCOB crystals possess the same crystal symmetry(space group C_m) to YCOB and its analogues. The lattice parameters were calculated and found to be a= 8.068 Å, b= 16.014 Å, c= 3.522 Å, and β= 101.11°, slightly lower than YCOB (PDF#50-0403: a = 8.078 Å, b = 16.022 Å, c = 3.534 Å and β = 101.19°), which is associated with the smaller ionic radius of Tm^{3+} (r^{Tm3+}=0.880 Å) than Y^{3+} (r^{Y3+}=0.890 Å). Based on the lattice parameters, the theoretical crystal density of TmCOB was calculated to be on the order of 3.88g/cm^3, similar to that obtained by the Archimedes method (3.91g/cm^3 at 25°C). Taking advantage of the four-circle diffractometer, the crystal structure of TmCOB was studied, where disorder distribution of Ca^{2+} and Tm^{3+} in TmCOB crystals were observed, from which the molecular formula of the grown TmCOB crystal was determined to be $(Tm_{0.78}Ca_{0.22})(Ca_{3.78}Tm_{0.22})O(BO_3)_3$.

3.4 Thermal expansion and thermal conductivity

For high temperature piezoelectric applications, thermal expansion coefficients and thermal conductivities are important parameters for device fabrication and design. As far as the monoclinic TmCOB crystals are concerned, there are four independent thermal expansion coefficients (α_{11}, α_{22}, α_{33} and α_{13}) due to the crystal symmetry, where the α_{11}, α_{22} and α_{33} can be obtained by measuring the thermal expansion along the physical *X*-, *Y*-, and *Z*-axes, respectively, according to the IEEE standard.[31]

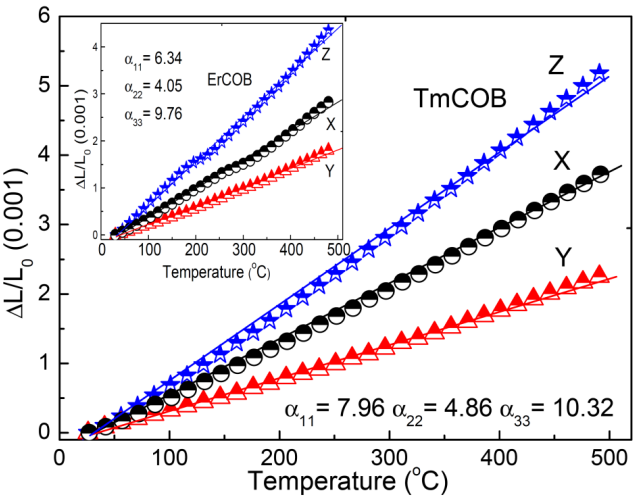

Fig. 3 Thermal expansion ratio curves for TmCOB crystals

Fig. 3 presents the measured thermal expansion curves for TmCOB crystal along different physical axes, from which the thermal expansion coefficients were determined to being on the order of α_{11}=7.96, α_{22}=4.86 and α_{33} =10.32×10^{-6}/°C, respectively, approximate to those of YCOB crystals (α_{11}=7.45, α_{22}=3.88 and α_{33}=10.43×10^{-6}/°C) but slightly higher than ErCOB crystals (α_{11}=6.34, α_{22}=4.05 and α_{33}=9.76×10^{-6}/°C), as presented in the small inset of Fig.3. The relatively larger expansion coefficients α_{33} and α_{11} than α_{22} were believed to be associated with the layered structure of ReCOB crystals parallel to the (-201) planes, where the average bonding strength perpendicular to the (-201) planes were relatively weak due to the large average bond length.[33]

Temperature dependence of the thermal conductivity (κ), thermal diffusivity(λ) and specific heat (C_p) along the physical *Y*-axis (crystallography *b*-axis) were characterized by using the laser pulse method for TmCOB crystals(parameters were measured at three different points of the sample under the same test temperature), results are shown in Fig. 4, together with ErCOB for comparison (small inset of Fig. 4). The thermal conductivity κ, thermal diffusivity λ and specific heat C_p were measured and found to be on the order of 2.17 W/(m·°C), 0.76mm^2/s and 0.73 J/(g·°C) at RT for TmCOB crystals, respectively, while 2.54W/(m·°C), 0.93mm^2/s and 0.71J/(g·°C) for ErCOB crystals, respectively. The specific heat values for TmCOB and ErCOB crystals were observed to slightly increase with increasing temperature from 20°C to 700°C, exhibiting variations being on the order of 31.8% and 40.6% for TmCOB and ErCOB, respectively. On the contrary, the thermal diffusivity λ values for TmCOB and ErCOB crystals were found to decrease with increasing temperature, showing negative variations being around -29.3% and -33.3%, respectively. Of interest is that the thermal conductivities (κ) for TmCOB and ErCOB crystals were found to show high temperature stability, with minimal variations of <-10% over the test temperature range.

Table I Thermal conductivity (κ) and thermal diffusivity (λ) along *X*-, *Y*- and *Z*- axes for TmCOB crystals.

Parameters	Orientations	28°C	300°C	500°C	700°C
C_p (J/(g·°C))	/	0.73	0.93	0.96	0.97
Diffusivity λ (mm^2/s)	X	0.64	0.42	0.36	0.37
	Y	0.76	0.62	0.53	0.54
	Z	0.88	0.59	0.49	0.51
Conductivity κ (W/(m·°C))	X	1.83	1.53	1.35	1.40
	Y	2.17	2.25	1.99	2.05
	Z	2.52	2.15	1.83	1.93

The anisotropy characteristics of thermal diffusivity and thermal conductivity of TmCOB crystals were summarized in Table I, where the largest thermal conductivity was found to be along *Z*-axis, being on the order of 2.52W/(m·°C) at room temperature, while slightly decreased to 1.93W/(m·°C) at 700°C.

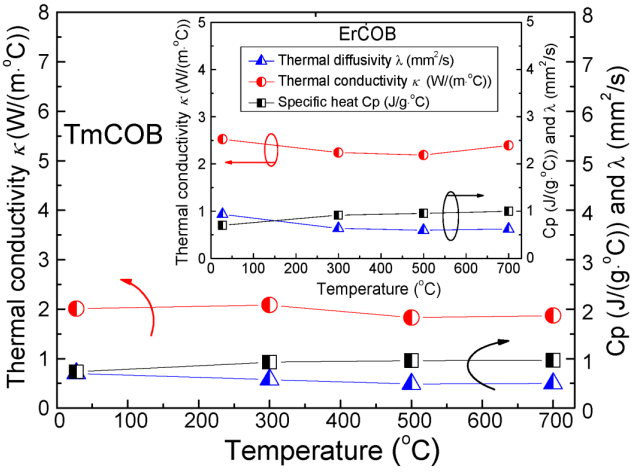

Fig. 4 Variation of the thermal conductivity κ, thermal diffusivity λ and specific heat C_p along *b*-axis as function of temperature

3.5 Electrical resistivity at elevated temperatures

Fig. 5 shows the temperature dependence of electrical resistivity ρ along the physical *X*-, *Y*- and *Z*-axes for TmCOB crystals, together with its analogue compound YCOB and structural ordered langasite type crystal $Ca_3TaGa_3Si_2O_{14}$ (CTGS) for comparison. As expected, the temperature dependent resistivities follow Arrhenius law over 500-900°C, where the activation energies (Ea) for TmCOB crystals were calculated and found to be 0.84eV, slightly higher than YCOB crystals (0.83eV) but lower than CTGS crystals (1.3eV), which is believed to be the ionic conduction for TmCOB crystals at elevated temperatures. In addition, the TmCOB crystals were found to possess relatively weak anisotropy of the electric resistivity, where the resistivity along the physical *X*-axis was measured to be slightly higher than that along physical *Y*- and *Z*-axes. The electric resistivity along *Y*-axis was measured to be on the order of $1\times10^7\Omega$·cm at 900°C, approximate to that of YCOB crystals ($4\times10^7\Omega$·cm),[24] being one order higher than CTGS crystals (~$1\times10^6\Omega$·cm at 900°C).

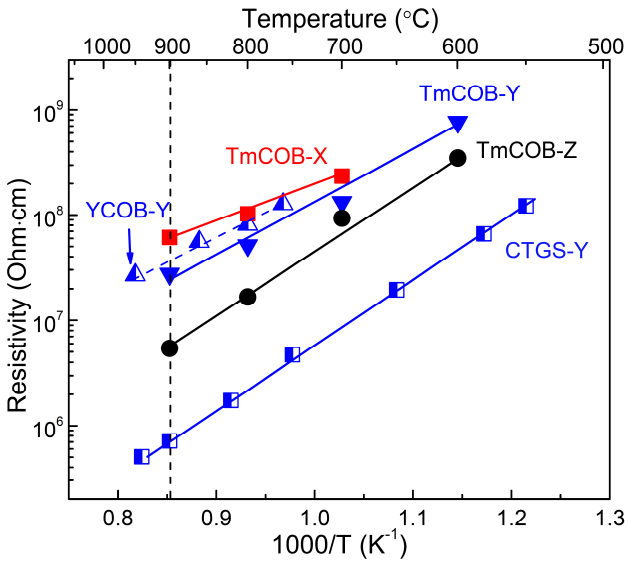

Fig. 5 Variation of electrical resistivity versus temperature for TmCOB crystals

3.6 Dielectric, elastic and piezoelectric properties at room temperature

The dielectric, elastic, and piezoelectric constants were evaluated taking advantage of the impedance method, according to the IEEE standard on piezoelectricity.[31] Various crystal cuts, including the rods, square plates and rectangular plates, were prepared for longitudinal, shear and transverse vibration modes investigations. Different to previous work, more crystal cuts with special designed rotation angles were prepared for electro-elastic constants determination. For each crystal cut, at least four specimens were prepared and measured to get the average value of dielectric, elastic and piezoelectric constants. Based on the measured capacitance and the observed resonance frequency (fr) and anti-resonance frequency (fa) for different TmCOB crystal cuts, the dielectric constant, elastic compliances and piezoelectric coefficients were obtained, referring to the procedures and equations for YCOB and NdCOB crystals.[29, 34]

Table II summarized the complete set of dielectric, elastic and piezoelectric constants for TmCOB crystals. Comparing to YCOB crystals, the dielectric constants for TmCOB crystals, being on the order of $\varepsilon^{T}_{11}/\varepsilon_0$=9.13, $\varepsilon^{T}_{22}/\varepsilon_0$=11.6 and $\varepsilon^{T}_{33}/\varepsilon_0$= 9.14, were slightly lower than YCOB crystals. It is noted that the elastic compliances, electromechanical coupling factors and piezoelectric coefficients are very close to YCOB crystals. Of particular interest, the piezoelectric coefficient d_{26}, which was verified utilizing the thickness shear vibration mode of *Y*-plates, was found to be on the order of 7.8 pC/N, slightly lower than that of YCOB crystals (7.9~8.0 pC/N), in consistent with the previous revealed structure-property relationships for ReCOB crystals,[24,29] where the elastic compliance s_{66}, dielectric constant $\varepsilon^{T}_{22}/\varepsilon_0$, electromechanical coupling factor k_{26}, piezoelectric coefficient d_{26} and mechanical quality factor Q_m for ReCOB crystals show strong dependence to the rare-earth ionic (Re^{3+}) radius. The smaller of the Re^{3+} radius, the lower piezoelectric d_{26}, and the higher electrical resistivity and mechanical quality factor the ReCOB may possess.

Table II Summary of the dielectric, elastic and piezoelectric constants for TmCOB crystals, together with YCOB crystals for comparison.

Elastic compliances s^{E}_{ij} (pm^2/N)													
	s_{11}	s_{12}	s_{13}	s_{15}	s_{22}	s_{23}	s_{25}	s_{33}	s_{35}	s_{44}	s_{46}	s_{55}	s_{66}
TmCOB	7.08	-0.56	-2.0	-0.62	6.85	0.05	1.1	8.94	-0.04	36.7	-0.45	20.4	16.4
YCOB[34]	7.2	-0.8	-2.47	-0.4	7.0	0.55	0.54	8.9	-0.12	34.5	-0.37	21.0	16.3
YCOB[35]	7.15	-0.35	-2.8	0.74	6.91	-0.68	-0.46	8.79	-1.2	35.0	3.5	23.0	15.0
Dielectric constants $\varepsilon^{T}_{ij}/\varepsilon_0$													
	ε_{11}	ε_{13}	ε_{22}	ε_{33}									
TmCOB	9.13	0.88	11.3	9.14									
YCOB[34]	9.65	0.95	11.8	9.55									
YCOB[35]	9.57	-0.96	11.4	9.52									
Piezoelectric coefficients d_{ij} (pC/N)													
	d_{11}	d_{12}	d_{13}	d_{15}	d_{24}	d_{26}	d_{31}	d_{32}	d_{33}	d_{35}			
TmCOB	1.7	3.8	-4.2	-0.92	4.9	7.8	-0.75	-2.4	2.2	-5.2			
YCOB[34]	1.7	3.9	-4.2	-1.1	4.4	7.9	-0.77	-2.5	1.4	-5.0			
YCOB[35]	1.4	3.8	-4.2	-7.2	-2.6	8.0	-0.22	-2.3	0.83	2.2			
Electromechanical coupling factors k_{ij} (%)													
	k_{11}	k_{12}	k_{13}	k_{15}	k_{24}	k_{26}	k_{31}	k_{32}	k_{33}	k_{35}			
TmCOB	7.0	15.4	14.2	2.1	8.1	19.2	3.2	10.5	8.3	12.8			
YCOB[34]	6.9	15.6	15.4	2.5	7.4	19.0	3.05	10.3	5.1	11.9			

* Dielectric constant for TmCOB was determined at 100 kHz, with dielectric loss <0.01%.

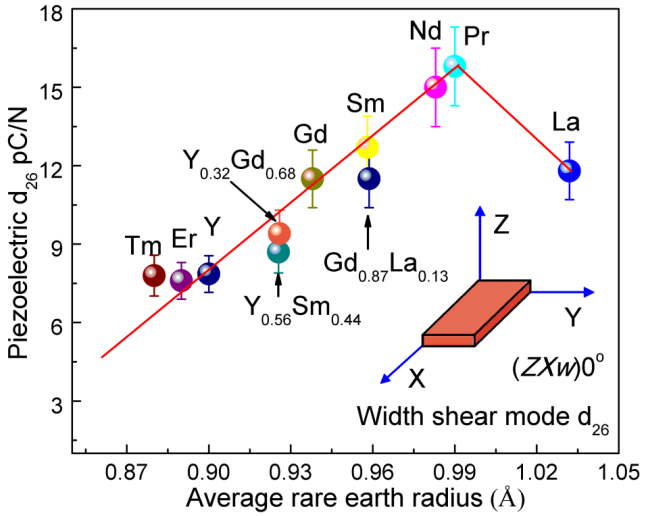

Fig. 6 Piezoelectric coefficient d_{26} as a function of rare-earth ionic radius (the average ionic radius for $Y_{0.56}Sm_{0.44}COB$, $Y_{0.32}Gd_{0.68}COB$ and $Gd_{0.13}La_{0.87}COB$ crystals were calculated to be 0.926 Å, 0.926 Å and 0.959Å, respectively.)

For further verification of the structure-property relationships in ReCOB crystals, piezoelectric coefficients d_{26} for the mixed $Re^{1}_{x}Re^{2}_{1-x}COB$ crystals, including $Y_xSm_{1-x}COB$, $Y_xGd_{1-x}COB$ and $Gd_xLa_{1-x}COB$ crystals with respectively actual composition of $Y_{0.56}Sm_{0.44}COB$, $Y_{0.32}Gd_{0.68}COB$ and $Gd_{0.13}La_{0.87}COB$ (determined by using the X-ray fluorescence method), were evaluated and found to be on the order of 8.7, 9.4 and 11.5 pC/N, respectively.

It is reasonable to confirm that the Re^{3+} contributed to the piezoelectric properties of ReCOB crystals, and the relative low piezoelectric d_{26} for TmCOB crystals is resulted from the relative small Re^{3+} radius,being on the order of $r^{Tm(3+)}$=0.88Å. Thus, high electrical resistivity (studied in section 3.5) and high mechanical quality factor for TmCOB are expected.

Fig. 6 plotted the variation of piezoelectric d_{26} as a function of Re^{3+} radius for various ReCOB type crystals, including the pure TmCOB, YCOB, GdCOB, SmCOB, NdCOB, PrCOB and LaCOB crystals, and mixed $Y_{0.56}Sm_{0.44}COB$, $Y_{0.32}Gd_{0.68}COB$ and $Gd_{0.13}La_{0.87}COB$ crystals. The measured piezoelectric coefficients d_{26} for the designed TmCOB crystals and the mixed $Y_{0.56}Sm_{0.44}COB$, $Y_{0.32}Gd_{0.68}COB$ and $Gd_{0.13}La_{0.87}COB$ crystals were in good agreement with the predicted trend, where the lowest piezoelectric d_{26} (7.8pC/N) was obtained for TmCOB, while the highest d_{26} value was observed for PrCOB crystals (15.8pC/N), associated with the distortion of Re-O octahedrons in ReCOB crystals.

3.7 Temperature dependence of dielectric, elastic and piezoelectric properties

For potential high temperature piezoelectric applications, temperature dependence of the dielectric, electromechanical and piezoelectric properties were investigated over the temperature range of 20°C-900°C. Fig.7 presents the temperature dependence of the dielectric constant and dielectric losses for TmCOB crystals, where the dielectric constant $\varepsilon^T_{11}/\varepsilon_0$, $\varepsilon^T_{22}/\varepsilon_0$ and $\varepsilon^T_{33}/\varepsilon_0$ were observed to increase with increasing temperature, from 9.13, 11.3 and 9.14 at room temperature to 11.5, 14.9 and 15.3 at 900°C, respectively. It is worth to notice that the dielectric losses $tan\delta_{11}$ and $tan\delta_{22}$ for TmCOB crystals were observed to slightly increase with increasing temperature, being on the order of ~21% at 900°C, much lower than $tan\delta_{33}$ (~85% at 900°C), which was found to sharply increase when the temperature go higher than 500°C. The high dielectric loss $\tan\delta_{33}$ at elevated temperature is believed to be associated with the relative low electrical resistivity (high electrical conductivity), as presented in Fig. 5.

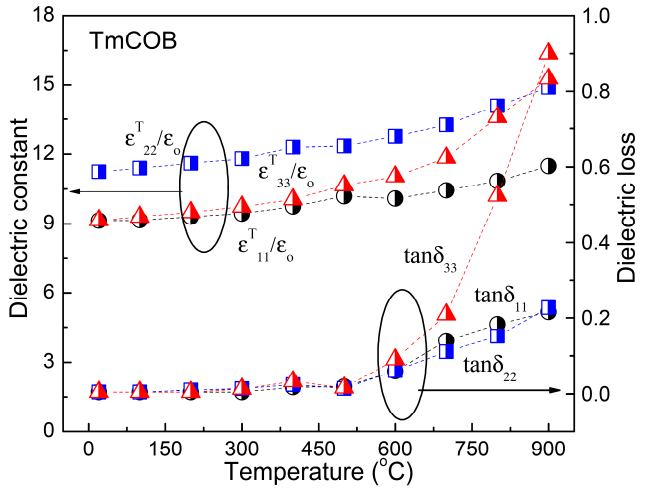

Fig. 7 Variations of the dielectric constant and dielectric loss as a function of temperature

The elastic compliances were studied by measuring the resonance and anti-resonance frequencies for different vibration modes, including the transverse modes d_{12} and d_{13}, and shear modes d_{35} and d_{26}, corresponding to the compliances s^E_{22}, s^E_{33}, s^E_{55} and s^E_{66}, respectively, as shown in the inset of Fig. 8. The shear mode d_{26} shows the largest |fa-fr| values being on the order of 7.5 kHz, leading to the largest electromechanical coupling factor k_{26} of 19.2%. In addition, the variations of elastic compliances s^E_{22}, s^E_{33}, s^E_{55} and s^E_{66} as a function of temperature were obtained, all this investigated elastic compliances increased dramatically with increasing temperature from RT to 900°C, due to the fact that resonance and anti-resonance shifted to lower frequency as increasing temperature, offering high variations being on the order of 16.7%, 19.6%, 19.2% and 13.4% for s^E_{22}, s^E_{33}, s^E_{55} and s^E_{66}, respectively.

Combining with the determined dielectric constant, resonance and anti-resonance frequencies, and elastic compliances at elevated temperatures, the temperature dependence of the electromechanical coupling factors k_{ij} and piezoelectric coefficients d_{ij} for TmCOB crystals were determined. Fig. 9 presents the variations of the electromechanical coupling factors and piezoelectric coefficients as a function of temperature, relating to the transverse d_{12} (k_{12}) and d_{13} (k_{13}), and shear d_{35} (k_{35}) and d_{26} (k_{26}), where TmCOB crystals were found to possess large difference of temperature dependent behaviors for the coupling k_{ij} and piezoelectric d_{ij}. Among the investigated electromechanical coupling factors, the transverse coupling k_{12}, which was determined to be on the order of 15.4% at RT, exhibited the highest temperature stability, leading to a minimal variation of 5.4% over the test temperature range, approximate to that of YCOB (variation of k_{12} being 4.5%).[36] However, the transverse coupling k_{13}, and shear coupling k_{26} and k_{35} exhibited different temperature dependent behaviors, with relative large variations being on the order of -10.9%, -16.7% and 21.8%, respectively.

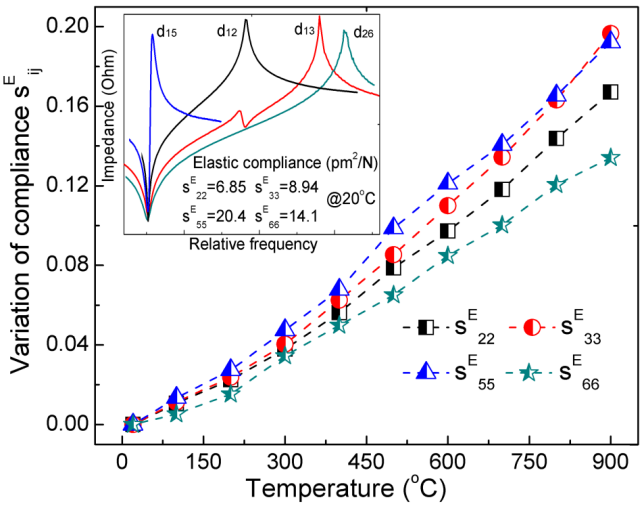

Fig. 8 Variations of the elastic compliances as a function of temperature

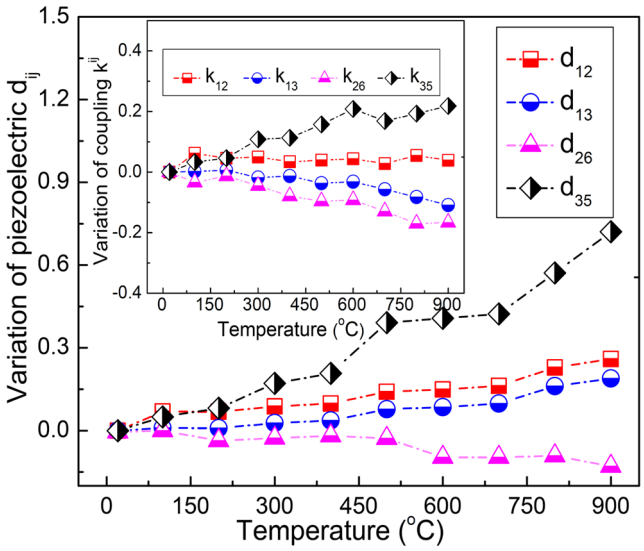

Fig. 9 Variation of piezoelectric coefficients d_{ij} and electromechanical coupling factors k_{ij} as a function of temperature

Similar to the coupling factor k_{ij}, the piezoelectric coefficient d_{ij} for TmCOB crystals varied differently with increasing temperature, exhibiting different temperature dependent behaviors. It was found

that the transverse piezoelectric coefficients d_{12} and d_{13} for TmCOB crystals slightly increased from 3.8 and -4.2pC/N at RT to 4.4 and -5.1pC/N at 900°C, showing relative large variations being on the order of 16.0% and 21.0%, respectively, while the shear piezoelectric d_{35} was observed to dramatically increase with increasing temperature, give a large variation being on the order of 75%. Of particular interest is that the piezoelectric coefficient d_{26} was obtained to show temperature independent property, with minimal vibration being on the order of 12.9% from RT to 900°C, much lower than that of YCOB crystals (variation >17%[37]), exhibiting the advantages for high temperature piezoelectric applications.

Conclusions

High temperature piezoelectric sensing requires the piezoelectric element possessing the merits of high electrical resistivity and low dielectric loss at elevated temperatures, high piezoelectric coefficient and high temperature stability of electromechanical and piezoelectric properties. In this paper, new piezoelectric crystals TmCOB were designed based on the structure-property relationships, and grown by using the Cz pulling method. For potential high temperature piezoelectric applications, thermal properties (thermal expansion and thermal conductivities) and electro-elastic properties were studied from RT to 900°C. The thermal expansion coefficients for TmCOB were measured to be α_{11}=7.96, α_{22}=4.86, and α_{33}= 10.32 (10^{-6}/°C), respectively. The specific heat and thermal conductivity at room temperature were obtained to be on the order of 0.73J/(g·°C) and 2.17W/(m·°C) (along *Y*-axis), changed to 0.97J/(g·°C) and 2.05W/(m·°C) (along *Y*-axis) at 700°C, respectively. Particularly, the TmCOB crystals were found to possess high electrical resistivity and low dielectric loss, being on the order of ρ_{11}=6×10^7Ω·cm and $tan\delta_{22}$<15% at 900°C, respectively. Moreover, TmCOB crystals exhibit high piezoelectric coefficient (d_{26}=7.8pC/N at RT), three times that of quartz, while maintaining the similar value up to 900°C, with minimal variation being on the order of <12.9%, all these properties demonstrate the advantages of TmCOB crystals for high temperature sensing applications.

Acknowledgements

This work was supported by the National Natural Science Foundation of China (Grant Nos. 91022034 and 51202129), and Natural Science Foundation of Shandong Province (ZR2012EMQ004).

Notes and references

[a] *Institute of Crystal Materials and State Key Laboratory of Crystal Materials, Shandong University, Jinan, 250100, China；E-mail: fapengyu@sdu.edu.cn; zhaoxian@icm.sdu.edu.cn. Fax: +86 531 88364864; Tel: +86 531 88364068*

[b] *Materials Research Institute, Pennsylvania State University, University Park, PA, 16802, USA*

[c] *School of Chemistry and Chemical Engineering, Shandong University, Jinan 250100, P.R. China State Key Laboratory of Crystal Materials, Shandong University, Jinan 250100, P.R. China*

[d] *Key Laboratory of Functional Crystal Materials and Device (Shandong University), Ministry of Education, Jinan 250100, China*

1 C. P. Christensen, *Science*, 1982, **218**, 115.

1 R. C.Turner, P. A. Fuierer, R. E. Newnham, *Appl. Acoust*., 1994, **41**, 299.

2 S. J. Zhang, F. P. Yu, *J. Am. Ceram. Soc.*, 2011, **94**, 3153.

3 H. Fritze, H. L. Tuller, *Appl. Phys. Lett.,* 2001, **78**, 976.

4 S. J. Zhang, X. N. Jiang, M. Lapsley, P. Moses, T. R. Shrout, *Appl. Phys. Lett.*, 2010, **96**, 013506.

5 D. Damjanovic, *Curr.Opin. Solid St. M.,* 1998, **3**, 469.

6 S. J. Zhang, Frantz, E. Xia, R. Everson, W. Randi, J. Snyder, D.W. Shrout, T. R. J. Appl. Phys. 2008, 104, 084103.

7 X. N. Jiang, K. Kim, S. J. Zhang, J. Johnson, G. Sakazar, *Sensors*, 2014, **14**, 144.

8 Q. Ye, B. H. T. Chai, *J. Cryst. Growth*, 1999, **197**, 228-235.

9 J. Wang, X. Hu, X. Yin, R. Song, J. Wei, Z. Shao, Y. Liu, M. Jiang, Y. Tian, J. Jiang, W. Huang, J. Mater. Res. 2001, 16, 790-796.

10 H. Shimizu, H. Takeda, T. Nishida, S. Okamura, T. Shiosaki, T. Shikida, *Proc.-IEEE Ultrason. Symp*., 2004, 1218.

11 H. Takeda, H. Sako, H. Shimizu, K. Kodama, M. Nishida, H. Nakao, T. Nishida, S. Okamura, T. Shikida, *Jpn. J. Appl. Phys.*,2003, **42**, 6081.

12 H. Shimizu, T. Nishida, M. Nishida, H. Takeda, T. Shiosaki *Jpn. Jpn. J. Appl. Phys.*, 2005, **44**, 7059.

13 A. H. Reshak, S. Auluck, I. V. Kityk, *J. Phys.: Condens. Matter*, 2008, **20**, 145209.

14 T. Lukasiewicz, J. Kisielewski, L. Lipinska, A. Majchrowski, G. Lakshminarayana, I. V. Kityk, *J. Alloys Compd.*, 2011, **509**, 3473.

15 A. H. Reshak, X. Chen, F. Song, I. V. Kityk, S. Auluck, *J. Phys.: Condens. Matter*, 2009,**21**, 205402.

16 A. H. Reshak, S. Auluck, I. V. Kityk, *J. Phys. Chem. A*, 2009,**113**, 1614-1622.

17 A. H. Reshak, S. Auluck, I. V. Kityk, *J. Phys. D: Appl. Phys.*, 2009, **42**, 085406.

18 E. Markiewicz, C. Z. Pawlaczyk, A. Kłos, W. Hofman, A. Pajączkowska, *Phys. Stat. Sol. (a),* 2006, **203**, 372.

19 S. J. Zhang, J. G. Zhang, Z. X. Cheng, G. Y. Zhou, J. R. Han, H. C. Chen, *J. Cryst. Growth*, 1999, **203**, 168.

20 H. Shimizu, K. Kodama, H. Takeda, T. Nishida, T. Shikida, S. Okamura, T. Shiosaki, S. Okamura, T. Shiosaki, *Jpn. J. Appl. Phys.,* 2004, **43**, 6716.

21 Y. T. Fei, B. H. T. Chai, C. A. Ebbers, Z. M. Liao, K. I. Schaffers, P. Thelin, *J. Cryst. Growth*, 2006, **290**, 301.

22 H. J. Zhang, H. D. Jiang, J. Y. Wang, X. B. Hu, G. W. Yu, W. T. Yu, L. Gao, J. A. Liu, S. J. Zhang, M. H. Jiang, *Appl. Phys. A.*, 2004, **78**, 889.

23 G. Aka, A. Kahn-Harari, F. Mougel, D. Vivien, F. Salin, P. Coquelin, P. Colin, D. Pelenc, J. P. Damelet, *J. Opt. Soc. Am. B*, 1997, **14**, 2238.

24 F. P. Yu, S. J. Zhang, X. Zhao, S. Y. Guo, X. L. Duan, D. R. Yuan, T. R. Shrout, *J. Phys. D: Appl. Phys.*, 2011, **44**, 135405.

25 K. Kim, S. J. Zhang, W. B. Huang, F. P. Yu, X. N. Jiang, *J. Appl. Phys.,* 2011, **109**, 126103.

26 K. Kim, S. J. Zhang, G. Salazar, X. N. Jiang, *Sensors Actuat. A: Phys.,* 2012, **178**, 40.

27 H. Nakao, M. Nishida, T. Shikida, H. Shimizu, H. Takeda, T. Shiosaki, *J. Alloys Compd.*, 2006, **408**, 582.

28 T. Karaki, M. Adachi, Y. Kuniyoshi, *J. Electroceram.*, 2008, **21**, 823.

29 F. P. Yu, S. J. Zhang, X. Zhao, D. R. Yuan, C. M. Wang, T. R. Shrout, *Cryst. Growth Des.*, 2010, **10**, 1871.

30 F. P. Yu, S. J. Zhang, X. Zhao, D. R. Yuan, L. F. Qin, M. W. Qing, T. R. Shrout, *IEEE T Ultrason. Ferr. Freq. Contr.*, 2011, **58**, 868.

31 IEEE Standard on Piezoelectricity. An American National Standard, 1987, vol.14.

32 A.B. Ilyukhin, B.F. Dzhurinskii, Russ. *J. Inorg. Chem.*,1993, **38**, 917.

33 Y. Q. Liu, L. Wei, F. P. Yu, Z. P. Wang, Y. G. Zhao, S. Han, X. Zhao, X. G. Xu, *CrystEngComm.*, 2013, **15** , 6035.
34 F. P. Yu, S. Hou, S. J. Zhang, Q. M. Lu, X. Zhao, *Phys. Stat. Sol. (a),* 2013, **211**, 574.
35 H. Shimizu, T. Nishida, H. Takeda, T. Shiosaki, *J. Cryst. Growth*, 2009, **311**, 916.
36 F. P Yu, S. Hou, X. Zhao, S. J. Zhang, I*EEE T Ultrason. Ferr. Freq. Contr.,* 2014, **61**, 1344.
37 F. P. Yu, S. J. Zhang, X. Zhao, D. R. Yuan, Q. M. Wang, T. R. Shrout, *Phys. Status Solidi-R.*, 2010, 5, 103-105.

